


Scaling of wetting and prewetting transitions on nanopatterned walls

Martin Pospíšil and Martin Láška 

*Department of Physical Chemistry, University of Chemical Technology Prague, Praha 6, 166 28, Czech Republic
and Department of Molecular and Mesoscopic Modelling, ICPF of the Czech Academy Sciences, Prague 16502, Czech Republic*

Andrew O. Parry

Department of Mathematics, Imperial College London, London SW7 2BZ, United Kingdom

Alexandr Malijevský*

*Department of Physical Chemistry, University of Chemical Technology Prague, Praha 6, 166 28, Czech Republic
and Department of Molecular and Mesoscopic Modelling, ICPF of the Czech Academy Sciences, Prague 16502, Czech Republic*



(Received 22 July 2019; published 3 September 2019)

We consider a nanopatterned planar wall consisting of a periodic array of stripes of width L , which are completely wet by liquid (contact angle $\theta = 0$), separated by regions of width D which are completely dry (contact angle $\theta = \pi$). Using microscopic density functional theory, we show that, in the presence of long-ranged dispersion forces, the wall-gas interface undergoes a first-order wetting transition, at bulk coexistence as the separation D is reduced to a value $D_w \propto \ln L$, induced by the bridging between neighboring liquid droplets. Associated with this is a line of prewetting transitions occurring off coexistence. By varying the stripe width L , we show that the prewetting line shows universal scaling behavior and data collapse. This verifies predictions based on mesoscopic models for the scaling properties associated with finite-size effects at complete wetting including the logarithmic singular contribution to the surface free energy.

DOI: [10.1103/PhysRevE.100.032801](https://doi.org/10.1103/PhysRevE.100.032801)

I. INTRODUCTION: WETTING AND BRIDGING TRANSITIONS

As first discussed by Cahn [1] and Ebner and Saam [2], a wetting transition refers to the vanishing of the contact angle θ of a liquid drop on a substrate (wall), say, as the temperature T is increased to a wetting temperature T_w —for reviews, see, for example, Refs. [3–5]. Equivalently, and more microscopically, the transition refers to the divergence of the thickness of the adsorbed layer of liquid at a planar wall-gas interface as T approaches T_w at bulk liquid-gas coexistence (chemical potential $\mu = \mu_{\text{sat}}$). This can also be thought of as the unbinding of the liquid-gas interface from the wall [6]. Wetting transitions can be continuous or first order depending on the sensitive balance and competition between the strength and the range of the wall-fluid and fluid-fluid intermolecular forces. In most situations, wetting transitions are first order in which case the thickness of the adsorbed liquid layer jumps from a microscopic to macroscopic value at T_w , that is, the liquid-gas interface unbinds discontinuously at T_w . Associated with this is a line of prewetting corresponding to first-order transitions between thin and thick adsorbed liquidlike layers when the bulk gas is undersaturated $\mu < \mu_{\text{sat}}$. On the T - $\delta\mu$ plane, where $\delta\mu = \mu_{\text{sat}} - \mu$, the line of prewetting transitions extends away tangentially from T_w and terminates at a prewetting critical point when the thin and thick phases become

indistinguishable [7]. First-order wetting transitions have been extensively studied both theoretically and experimentally.

When the wall is geometrically sculpted or chemically patterned the fluid adsorption can exhibit a zoo of new possibilities [8–17]. Attempts to understand this date back to the empirical work of Wenzel [18] (for sculpted or rough surfaces) and Cassie [19] for chemically patterned (planar) walls. For example, Cassie’s “law” states that the effective contact angle θ_{eff} on a composite substrate formed of two different materials with different contact angles θ_1 and θ_2 satisfies $\cos \theta_{\text{eff}} = f \cos \theta_1 + (1 - f) \cos \theta_2$ where f and $(1 - f)$ are the fractions of the respective wall areas of the different materials. However, more recent studies have shown that the situation is considerably richer due to new phase transitions, absent in this simple empirical picture, which are induced by the nanopatterning of the substrate. For example, when two semi-infinite materials meet at a line, a prewetting transition on either side can induce the lateral growth of a thick wetting layer which continuously spreads out across the surface [20]. Transitions also occur when a partially wet surface ($\theta > 0$) is decorated with stripes of a material which is completely wet ($\theta = 0$). When the distance D between the stripes is large separate liquid drops nucleate above each stripe. Analysis based on mesoscopic interfacial Hamiltonian models predict that, for systems with long-ranged dispersion forces, the maximum (midpoint) height of the drop scales at bulk coexistence as $h_m \propto \sqrt{L}$ where L is the strip width [21]. However, as the interstrip distance D is reduced, a single (larger) drop forms which spans both stripes and the

*malijevsky@icpf.cas.cz

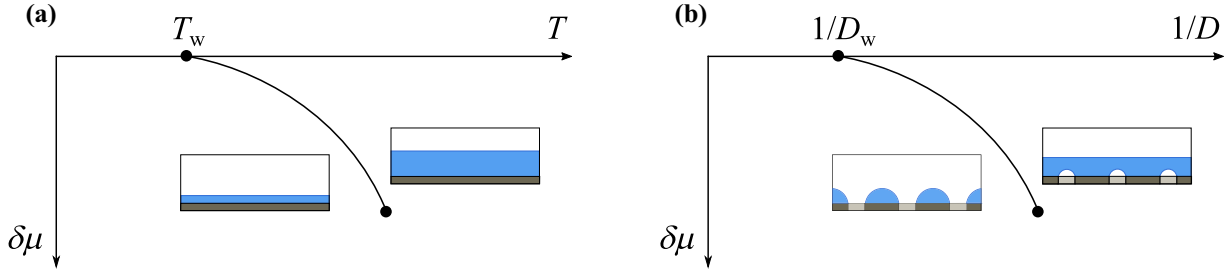


FIG. 1. Schematic surface phase diagrams representing first-order wetting transition (a) on a homogenous wall at a temperature T_w and (b) on a periodically nanopatterned wall of wet and dry stripes occurring when the distance D between the wet stripes is reduced to a value of D_w . Also shown are the prewetting lines extending tangentially from the wetting transition off coexistence $\delta\mu > 0$ which terminate at a prewetting critical point. A schematic of the phases which coexist along the prewetting line is also shown.

area between them. For systems with long-ranged forces, this bridging transition is predicted to occur when $D \propto \ln L$ which is always a molecularly short distance. The logarithmic dependence here directly arises from the finite-size contribution to the surface free energy of a drop above a completely wet stripe.

There is, in fact, a close connection between bridging and wetting transitions [22]. Consider, for example, a generalization of the above scenario where N completely wet stripes decorate a partially wet substrate in contact with a gas at bulk coexistence. Again, when the distance D between the stripes is long, each nucleates a separate liquid drop above it. As D is reduced to a value close to $\ln L$, there is a first-order phase transition to a single droplet which spans all the stripes and intervening (partially wet) spaces. For systems with dispersion forces, the height of this single large drop scales as $h_m \propto \sqrt{NL}$. It follows that in the limit $N \rightarrow \infty$, corresponding to a periodic array of stripes, the bridging transition is equivalent to the unbinding of a liquid-gas interface from the wall, i.e., a first-order wetting transition. There are several aspects of this structurally induced wetting transition which are of interest. First, it is driven by microscopic forces and is not captured by the approximate Cassie equation which predicts that $\theta_{\text{eff}} = 0$ only occurs when $f = 1$ (i.e., when the distance between the stripes regions vanishes). Second, if there is a first-order wetting transition when $D = D_w \propto \ln L$, then there should be a line of transitions analogous to prewetting occurring off coexistence for $D < D_w$ where a phase consisting of isolated drops coexist with a liquid film of finite thickness which covers the whole substrate. We illustrate this in Fig. 1(b) for the extreme scenario when the regions between the stripes are completely dry ($\theta = \pi$). In this case, the low adsorption phase consists of isolated liquid drops covering the wet stripes whereas the high adsorption phase has bubbles over the dry regions and an additional liquid-gas interface separating the liquid slab from the bulk gas. Now, if there is a prewetting line, then we should expect that it terminates at a prewetting critical point where the coexisting low and high adsorption phases are indistinguishable. However, if this is the case, we are left with the question as to how the two phases as sketched in Fig. 1 become indistinguishable since they appear to be structurally different. To understand this, we must abandon mesoscopic approaches which rely on simple pictures of interfacial configurations and apply fully microscopic theory based on molecular density profiles. The

purpose of the present paper is to study such bridging induced wetting and prewetting transitions using microscopic density functional theory (DFT). In addition to demonstrating that these transitions take place, we also show, by varying the stripe width L , that the locations of the prewetting lines show simple scaling data collapse associated with the presence of dispersion forces.

II. DENSITY FUNCTIONAL MODEL

Within the framework of classical DFT [23], the equilibrium density profile $\rho_{\text{eq}}(\mathbf{r})$, is obtained from the minimization of a grand potential functional $\Omega[\rho]$. This is exactly written

$$\Omega[\rho] = \mathcal{F}[\rho] + \int d\mathbf{r} \rho(\mathbf{r})[V(\mathbf{r}) - \mu], \quad (1)$$

where $V(\mathbf{r})$ is the external potential modeling the wall and $\mathcal{F}[\rho]$ is the intrinsic Helmholtz free-energy functional which contains all the information about the fluid-fluid intermolecular interaction. The formulation of DFT is exact, in principle, and higher derivatives of the free-energy functional determine direct correlation functions and, in turn, pairwise density-density correlations from the solution of the inhomogeneous Ornstein-Zernike equation. In most applications of DFT, approximations for $\mathcal{F}[\rho]$ must be performed. Varieties of these have been developed extensively over the past few decades to accurately model short-ranged intermolecular repulsive forces and long-ranged intermolecular attractions. It is standard to separate the Helmholtz free energy into an exact ideal gas contribution and an excess part,

$$\mathcal{F}[\rho] = \beta^{-1} \int d\mathbf{r} \rho(\mathbf{r})[\ln(\rho(\mathbf{r})\Lambda^3) - 1] + \mathcal{F}_{\text{ex}}[\rho], \quad (2)$$

where Λ is the thermal de Broglie wavelength and $\beta = 1/k_B T$ is the inverse temperature. Most modern DFT approaches follow the spirit of van der Waals, and the excess part is modeled as a sum of hard-sphere and attractive contributions where the latter is treated in simple mean-field fashion:

$$\mathcal{F}_{\text{ex}}[\rho] = \mathcal{F}_{\text{hs}}[\rho] + \frac{1}{2} \iint d\mathbf{r} d\mathbf{r}' \rho(\mathbf{r})\rho(\mathbf{r}')u_a(|\mathbf{r} - \mathbf{r}'|), \quad (3)$$

where $u_a(r)$ is the attractive part of the fluid-fluid interaction potential.

The fluid atoms are assumed to interact with one another via the truncated (i.e., short-ranged) and nonshifted

Lennard-Jones-like potential,

$$u_a(r) = \begin{cases} 0, & r < \sigma, \\ -4\varepsilon\left(\frac{\sigma}{r}\right)^6, & \sigma < r < r_c, \\ 0, & r > r_c. \end{cases} \quad (4)$$

which is cut off at $r_c = 2.5\sigma$, where σ is the hard-sphere diameter.

The hard-sphere part of the excess free energy is approximated using the fundamental measure theory functional [24],

$$\mathcal{F}_{\text{hs}}[\rho] = \frac{1}{\beta} \int d\mathbf{r} \Phi(\{n_\alpha\}), \quad (5)$$

which accurately takes into account the short-range correlations between fluid particles allowing for an accurate description of layering arising from the volume exclusion when a high density liquid is in contact with a wall. We have adopted the original Rosenfeld theory where there are six weighted densities n_α which are themselves convolutions of the density profile and fundamental measures of the hard sphere of diameter σ .

The external potential $V(\mathbf{r})$ is chosen to model a periodic array of stripes of width L separated by regions of width D . Here, $\mathbf{r} = (x, z)$ where x and z are the coordinates along and perpendicular to the wall, respectively. Translational invariance is assumed along the stripes, and the potential is infinite for $z < 0$, i.e., a hard-wall repulsion. However, in the stripe regions, we assume that there is a strong attraction between the fluid particles and the substrate atoms which are assumed to be uniformly distributed with density ρ_w . The potential $V(\mathbf{r})$ for $z > 0$ is then determined by integrating $\rho_w \phi_w(r)$ over the volume of the whole array of stripes. Here, $\phi_w(r)$ is the long-ranged attractive tail of the Lennard-Jones potential,

$$\phi_w(r) = -4\varepsilon_w \left(\frac{\sigma}{r}\right)^6, \quad (6)$$

which has a strength parameter ε_w chosen to emulate complete wetting if the striped region covered the whole surface. Hence, the attractive part of the wall potential can be written as

$$V(x, z) = \sum_{n=-\infty}^{\infty} V_L(x + nL, z), \quad (7)$$

where

$$V_L(x, z) = \alpha_w \left[\frac{1}{(x-L)^3} - \frac{1}{x^3} + \psi_6(x-L, z) - \psi_6(x, z) \right], \quad (8)$$

with

$$\alpha_w = -\frac{1}{3}\pi\varepsilon_w\sigma^6\rho_w, \quad (9)$$

and

$$\psi_6(x, z) = -\frac{2x^4 + x^2z^2 + 2z^4}{2z^3x^3\sqrt{x^2 + z^2}}. \quad (10)$$

In our substrate model, the region in between the stripes is modeled by a simple hard-wall potential meaning that these parts of the substrate would be completely dry at any temperature if they were of macroscopic extent. In our calculations,

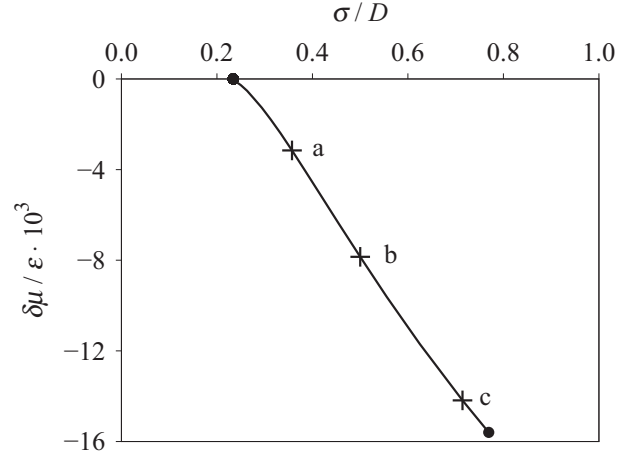


FIG. 2. Numerical DFT results showing the locations of the wetting and prewetting transitions on a dry hard wall patterned with completely wet stripes of width $L = 30\sigma$.

we have chosen $\varepsilon_w = \varepsilon$ for which the wetting temperature of the homogenous wall $T_w = 0.8T_c$ where T_c is the bulk critical temperature. By choosing $T = 0.92T_c$, we, therefore, ensure that the stripes are completely wet by liquid.

Minimization of (1) leads to the Euler-Lagrange equation,

$$V(\mathbf{r}) + \frac{\delta\mathcal{F}_{\text{hs}}}{\delta\rho(\mathbf{r})} + \int d\mathbf{r}' \rho(\mathbf{r}') u_a(|\mathbf{r} - \mathbf{r}'|) = \mu, \quad (11)$$

which can be solved iteratively on an appropriately discretized two dimensional (2D) grid $(0, x_m) \times (0, z_m)$ where $x_m = L + D$ represents one period and $z_m = 50\sigma$. Periodic boundary conditions are assumed at the edges in the x direction, and the density far from the wall at $z_m = 50\sigma$ is fixed to the equilibrium bulk vapor.

III. RESULTS: SCALING OF THE PREWETTING LINES

Figure 2 shows the numerically determined phase diagram for a patterned wall with stripes of width $L = 30\sigma$. As anticipated, at bulk coexistence, the system shows a first-order wetting transition at $D_w = 4.27\sigma$ at which a low adsorption phase consisting of isolated drops coexists with a completely wet state where a macroscopic layer of liquid covers the surface. The value of D_w is determined by balancing the grand potentials of these configurations, equivalent to an application of Antonoff's rule $\gamma_{\text{wg}} = \gamma_{\text{wl}} + \gamma$ which determines the contact angle on the substrate $\theta_{\text{eff}} = 0$. Here, γ_{wg} is the surface tension of the wall-gas interface (with droplets of liquid over the stripes), γ_{wl} is the surface tension of the wall-liquid interface (with bubbles of gas over the dry interstitial gaps), and γ is the usual liquid-gas surface tension of a planar interface. A similar matching of grand potentials determines the prewetting line extending away tangentially on the $1/D - \delta\mu$ plane. Representative coexisting densities are shown in Fig. 3. Close to bulk coexistence, we can easily distinguish drop and bubblelike structures which cover the wet or dry patches, respectively [see Fig. 3(a)]. However, on approaching the prewetting critical point, the value of the stripe separation D is so small that one can no longer detect bubble configurations

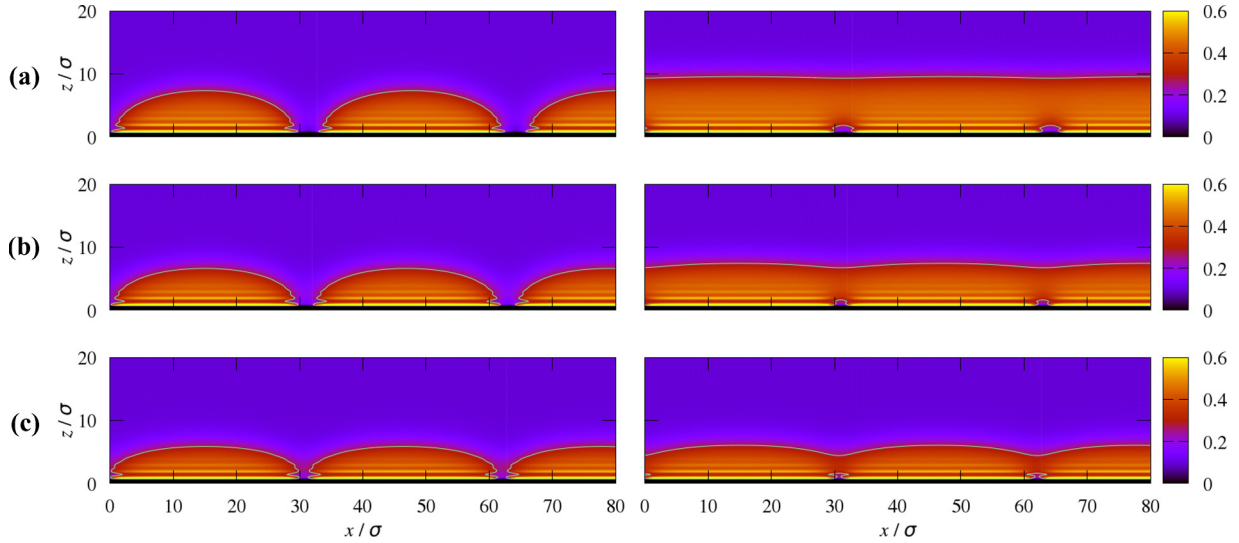


FIG. 3. Coexisting density profiles at three representative points along the prewetting for $L = 30\sigma$ as highlighted in Fig. 2. Close to bulk coexistence, the coexisting phases are structurally different, and droplets and bubbles over the wet and dry stripes can be distinguished. However, on approaching the prewetting critical point, the interfacial structure very close to the wall near the dry regions becomes more diffuse, and the phases become increasingly similar.

over the dry patches so that the density close to the wall is similar for both thin and thick film phases. That is, they become more and more structurally similar. At the prewetting critical point, the total adsorption $\Gamma = \int dx dz [\rho(\mathbf{r}) - \rho_g]$ is the same for both phases.

Finally, in Fig. 4(a), we show the phase diagrams obtained for five different stripe widths $L = 10\sigma, 20\sigma, 30\sigma, 40\sigma$, and 50σ expressed simply on the D - $\delta\mu$ plane. All the prewetting lines have a similar shape, and it is apparent that, as L increases, the value of D_w increases. In fact, we should anticipate that there is some data collapse which encapsulates universal features. Recall that for dispersion forces, the Clausius-Clapeyron equation determines that, close to bulk coexistence, the prewetting line $T_{pw}(\delta\mu)$ behaves as $T_w - T_{pw} \propto (\delta\mu)^{2/3}$ [3]. Here, the power-law dependence reflects the singular contribution to the excess surface free energy associated with the complete wetting transition. The constant of proportionality missing here is nonuniversal, system dependent, and related to the value of the Hamaker constant. A similar result applies to the present heterogeneous system, and all the prewetting lines $D_{pw}(\delta\mu)$ behave, close to bulk coexistence, as $D_{pw} - D_w \propto (\delta\mu)^{2/3}$. In fact, the only difference between prewetting curves shown in Fig. 4(a) is due to the stripe width L —otherwise, the systems are chemically identical. It follows that, if we rescale D and $\delta\mu$ allowing for their dependence on the stripe width L , there should be some data collapse. Figure 4(b) shows the data collapse obtained when D is rescaled with $\ln L/\sigma$ (as predicted for the value of D_w) and $\delta\mu$ by $L^{1/2}$ (representing the height of the droplets equivalent to their volume per unit area). Apart from the very smallest system $L = 10\sigma$, there is excellent data collapse for the shape of the prewetting line particularly close to bulk coexistence. This, therefore, verifies the predictions that the wetting transition occurs at $D_w \propto \ln L$ and that the droplet height scales as $h_m \propto \sqrt{L}$. This is the main finding of our paper.

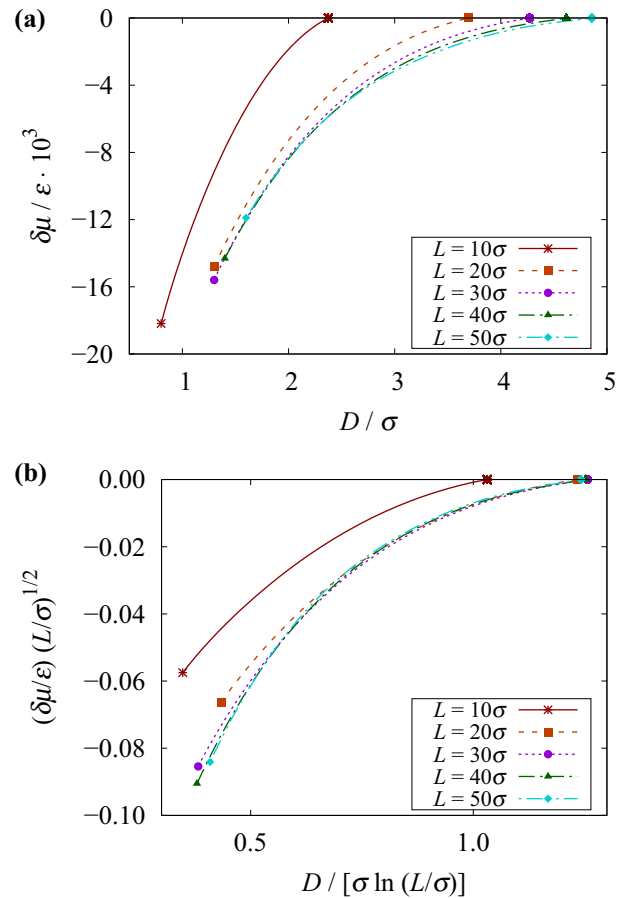


FIG. 4. Numerical DFT results showing (a) the wetting and prewetting lines for five different stripe widths and (b) the data collapse when the separation distance D and chemical potential field $\delta\mu$ are rescaled by $\ln L/\sigma$ and $\sqrt{L/\sigma}$, respectively.

IV. CONCLUDING REMARKS

Our paper has been based on a microscopic but mean-field DFT model which misses some fluctuation effects. However, unlike the bridging transition between two (or any finite number) of stripes, which beyond mean-field would be rounded by fluctuations, the wetting and prewetting transitions considered here remain genuine first order as predicted by mean-field theory. The present analysis should, therefore, accurately predict the value of the stripe spacing D_w where the wetting transition occurs. Second, the scaling dependence seen in the data collapse for the different prewetting lines is unchanged by interfacial fluctuations since they arise from critical singularities associated with complete wetting, the upper critical dimension for which is less than three for dispersion forces [6]. The only inaccuracy in the DFT analysis concerns predictions for the prewetting critical point which, beyond mean field, should belong to the true 2D Ising bulk universality class [25]. An interesting extension of the present paper would be to consider arrays of stripes with different widths which could lead to additional bridging transitions and the sequential coalescence of drops which precede a wetting transition. It would also be interesting to consider the effect of

disorder by randomizing the stripe widths, which would more realistically model experimental situations. Finally, it might be worth investigating the effect of the model fluid potential, e.g., by considering a long-ranged fluid-fluid potential, we expect much stronger interaction between the neighboring droplets facilitating their coalescence.

To summarize, we have used a microscopic DFT to demonstrate that bridging induced wetting transitions occur on nanopatterned walls comprising wet and dry stripes. The associated prewetting lines occurring in systems with different stripe widths show a simple data collapse which confirms scaling predictions for the height and finite-size surface free energy for complete wetting drops.

ACKNOWLEDGMENTS

This work was funded, in part, by the EPSRC UK Grant No. EP/L020564/1, “Multiscale Analysis of Complex Interfacial Phenomena.” A.M. acknowledges support from the Czech Science Foundation, Project No. GA17-25100S. M.P. acknowledges financial support from specific university research (MSMT Grant No. 21-SVV/2019).

-
- [1] J. W. Cahn, *J. Chem. Phys.* **66**, 3667 (1977).
 - [2] C. Ebner and W. F. Saam, *Phys. Rev. Lett.* **38**, 1486 (1977).
 - [3] S. Dietrich, in *Phase Transitions and Critical Phenomena*, edited by C. Domb and J. L. Lebowitz (Academic, New York, 1988), Vol. 12.
 - [4] M. Schick, in *Liquids and Interfaces*, edited by J. Chorvolin, J. F. Joanny, and J. Zinn-Justin (Elsevier, New York, 1990).
 - [5] D. Bonn, J. Eggers, J. Indekeu, J. Meunier, and E. Rolley, *Rev. Mod. Phys.* **81**, 739 (2009).
 - [6] G. Forgacs, R. Lipowsky, and T. M. Nieuwenhuizen. in *Phase Transitions and Critical Phenomena*, edited by C. Domb and J. L. Lebowitz (Academic, London, 1991), Vol. 14.
 - [7] E. H. Hauge and M. Schick, *Phys. Rev. B* **27**, 4288 (1983).
 - [8] M. Napiorkowski, W. Koch, and S. Dietrich, *Phys. Rev. A* **45**, 5760 (1992).
 - [9] A. O. Parry, C. Rascón, and A. J. Wood, *Phys. Rev. Lett.* **85**, 345 (2000).
 - [10] C. Bauer, T. Bieker, and S. Dietrich, *Phys. Rev. E* **62**, 5324 (2000).
 - [11] A. O. Parry, C. Rascón, N. B. Wilding, and R. Evans, *Phys. Rev. Lett.* **98**, 226101 (2007).
 - [12] A. Malijevský, *J. Chem. Phys.* **137**, 214704 (2012).
 - [13] A. Malijevský and A. O. Parry, *Phys. Rev. Lett.* **110**, 166101 (2013).
 - [14] A. Malijevský and A. O. Parry, *J. Phys.: Condens. Matter* **26**, 355003 (2014).
 - [15] A. O. Parry, A. Malijevský, and C. Rascón, *Phys. Rev. Lett.* **113**, 146101 (2014).
 - [16] A. Malijevský, *Phys. Rev. E* **99**, 040801(R) (2019).
 - [17] W. Tewes, O. Buller, A. Heuer, U. Thiele, and S. V. Gurevich, *J. Chem. Phys.* **146**, 094704 (2017).
 - [18] R. N. Wenzel, *Ind. Eng. Chem.* **28**, 988 (1936).
 - [19] A. B. D. Cassie, *Discuss. Faraday Soc.* **3**, 11 (1948).
 - [20] P. Yatsyshin, A. O. Parry, and S. Kalliadasis, *J. Phys.: Condens. Matter* **28**, 275001 (2016).
 - [21] A. Malijevský, A. O. Parry, and M. Pospíšil, *Phys. Rev. E* **96**, 032801 (2017).
 - [22] A. Malijevský, A. O. Parry, and M. Pospíšil, *Phys. Rev. E* **99**, 042804 (2019).
 - [23] R. Evans, *Adv. Phys.* **28**, 143 (1979).
 - [24] Y. Rosenfeld, *Phys. Rev. Lett.* **63**, 980 (1989).
 - [25] H. Nakanishi and M. E. Fisher, *Phys. Rev. Lett.* **49**, 1565 (1982).